ELSEVIER

Physica D 113 (1998) 1–25

PHYSICA D

Power spectra and dynamical invariants for delay-differential and difference equations

Boualem Mensour, André Longtin *

Département de Physique, Université d'Ottawa, 150 Louis Pasteur, Ottawa, Ont., Canada K1N 6N5

Received 1 February 1997; received in revised form 21 July 1997; accepted 21 July 1997
Communicated by A.M. Albano

Abstract

The Mackey–Glass and Ikeda delay-differential equations (DDEs) are models of feedback systems in which attractor dimension is proportional to the delay. Power spectra from these models are investigated analytically and numerically. As the delay increases much beyond the system response time, an exponentially decaying spectrum with a near-periodic superimposed modulation appears. It is shown that each peak in this modulation is associated with a mode of oscillation predicted by linear stability analysis around the fixed point. The number of such modes within a characteristic autocorrelation time of the solution agrees with the Lyapunov dimension of the attractor. The disappearance of this modulation at higher delay values is also explained. The decay rate of the spectrum in the mid-to-high frequency range is found to agree with the sum of the positive Lyapunov exponents, i.e. with the metric entropy. Realistic models with a distribution of delays display similar spectra as their memory kernel narrows into a delta-function. For very large delay, the DDE approaches an infinite-dimensional continuous-time difference equation (CTDE), with each point on a delay interval evolving independently and according to a chaotic discrete-time map. CTDE spectra, which have many features of finite-delay DDE spectra, can be computed analytically if the spectrum of this map is known. For constant initial functions, they have a $1/f^2$ form at low frequencies. Our analysis suggests that the spectrum of the chaotic map is at the origin of the peak shapes in DDE spectra at low frequency. Our findings highlight the relevance of the linear properties of DDEs to the characterization of their nonlinear properties.

Keywords: Delay-differential equations; Difference equations; Power spectra; Chaotic attractors; Mackey–Glass equation; Ikeda equation; Lyapunov dimension; Singular perturbation

1. Introduction

Delay-differential equations (DDEs) are used to model a large variety of nonlinear phenomena in which the time evolution depends not only on present states but also on states at or near a given time in the past (see e.g. [1] and references therein). From the point of view of nonlinear dynamics, these infinite-dimensional dynamical systems

* Corresponding author. Tel.: 613-562-5800 x6762; fax: 613-562-5190; e-mail: andre@physics.uottawa.ca.

0167-2789/98/$19.00 Copyright © 1998 Elsevier Science B.V. All rights reserved
PII S0167-2789(97)00185-1

are interesting because their chaotic attractors have a finite dimension proportional to the delay [2–5], making them useful to study general properties of high-dimensional chaos (Fig. 1). The large delay case, or more precisely, the large delay-to-response time case, has received a lot of attention because it is in this limit that certain properties of the DDE can be studied using a discrete-time map [6,7]. Other recent studies have approached the problem of high-dimensional chaos in DDEs through the use of interval maps [8] and iterative delay maps [9,10]. Further, there has been recent interest in DDEs at large delay in the context of phase defects and phase turbulence in lasers, which can be studied by arranging temporal solutions in a two-dimensional space–time representation [11].

DDEs at large delay are also of interest because they exhibit multistability, i.e. different initial conditions lead to different asymptotic periodic or chaotic solutions [12]. This property makes delay-differential systems attractive for memory storage purposes, as first suggested by Ikeda and Matsumoto [6]. In fact, it has been shown [13,14] that finite bit strings can be stored as specific periodic solutions of DDEs through judicious choices of initial conditions. The procedure works also for unstable periodic solutions stabilized by chaos-control techniques [15]. There has been much progress in our understanding of multistability and chaos in DDEs (see e.g. [6]), despite two main difficulties that hamper such studies. The first is that initial conditions for DDEs are functions on the delay interval $(-\tau, 0)$, where τ is the delay; evolution in functional spaces is more difficult to study than in finite-dimensional phase spaces. Further, calculating dynamical invariants for high-dimensional chaos is numerically very involved.

In this paper, we show that properties of DDEs at large delays, such as dynamical invariants and multistability, can in fact be studied using linear stability analysis, power spectra of temporal solutions, and a discrete-time map obtained from the DDE. Some of our results complement those in a recent paper [16] which suggested a relationship between, on the one hand, the exponential decay rate of such spectra, and on the other, the sum of certain Lyapunov exponents and thus the Lyapunov dimension. Our study makes use of two classes of dynamical systems obtained in the singular perturbation limit of the DDE [6,17]: the usual discrete-time one-dimensional map, as well as an infinite-dimensional continuous-time difference equation (CTDE). We find that the extreme multistability displayed by the CTDE, which is relevant to understanding memory storage and chaos control onto desired patterns in DDEs, can be exploited to explain features of large-delay spectra in DDEs, such as peak shapes. CTDE spectra can also be used to estimate attractor dimension in a corresponding DDE at mid-to-large delays.

The main advantage of working with spectra is that they are much simpler to calculate numerically compared to usual invariants, especially when the attractors are high-dimensional; the further advantage of working with CTDEs is that their spectra can be calculated analytically, once the spectrum of the aforementioned discrete-time map is determined (an even simpler numerical task).

An initial motivation for our work is an observation by Farmer [2] in his seminal study of dynamical invariants of DDEs. He noted in the power spectrum of the Mackey–Glass equation "a curious modulation" superimposed on an exponentially decaying envelope when the ratio R of delay-to-response time was large (30 in his study). We find that both the Ikeda and Mackey–Glass models exhibit such a near-periodic modulation when R is large, and that the peaks of this modulation are associated with the modes predicted by linear stability analysis of the dynamics around the fixed point. This correspondence in turn suggests new relationships between these linear modes, the spectral decay rate, the Lyapunov exponents and the Lyapunov dimension of the attractor. In particular we find that, at least for such first-order DDEs at large R values, the exponential decay rate observed at mid-to-high frequencies is more relevant to the characterization of dynamical invariants than the asymptotic spectrum (i.e. at very high frequency). This follows from the fact that most of the energy of the chaotic fluctuations lies in this frequency range, and is associated with the largest Lyapunov exponents and most unstable linear modes.

This paper is organized as follows. In Section 2, we discuss the properties of power spectra at different delays and over different frequency ranges, and introduce the CTDE and discrete-time map obtained in the singular perturbation limit of the DDE. The spectra are further characterized using notions from linear filter theory. In Section 3, we calculate the frequencies of the modes using linear stability analysis around the fixed point and associate them with

peaks in the power spectrum. Section 4 estimates the attractor dimension from the number of peaks in the power spectrum, and the sum of positive Lyapunov exponents from the rate of decay of the spectrum. It also discusses the spectra for the distributed delay case where the DDE is approximated by a finite number of ODEs. Section 5 gives a derivation of spectral properties of CTDE solutions for piecewise constant initial functions. It further discusses the connection between spectra of such unstable solutions, those of the singular limit map, and those of finite-delay DDEs. The paper concludes in Section 6.

2. Power spectra at different delays

2.1. Temporal behavior

First-order nonlinear DDEs such as Mackey–Glass or Ikeda equations have the form

$$\frac{\mathrm{d}x(t)}{\mathrm{d}t} = -bx(t) + F(x(t-\tau)). \tag{1}$$

To solve such an equation, it is necessary to specify the initial condition of x over one delay interval τ, i.e. one must specify an initial function. Since the domain of definition of a function is infinite, these dynamical systems are infinite-dimensional. In numerical simulations, we partition this delay interval into M subintervals. Thus the behavior of the infinite-dimensional DDE is approximated by that of an M-dimensional discrete dynamical system [2], which maps the values of x over one delay interval into those over the following delay interval. Fig. 1 shows numerical solutions of the Mackey–Glass equation [18] for different delays:

$$\frac{\mathrm{d}x(t)}{\mathrm{d}t} = -bx(t) + \frac{ax(t-\tau)}{1+x^{10}(t-\tau)}. \tag{2}$$

The parameters chosen [2,16], $a = 0.2$, $b = 0.1$, are the same throughout our study. A fourth-order Runge–Kutta method with linear interpolation on the delay variable has been used throughout our study. As the ratio $R = \tau/\tau_r$ of the delay-to-response time $\tau_r = 1/b$ increases, the chaotic solution loses some of its regularity, as can be seen on going from Figs. 1(a) to (b). For very large R values (Fig. 1(c): $R = 500$), the solution which evolves from a constant initial condition exhibits plateaus, with a bit of chaotic fluctuations at the end of each plateau. In the singular limit $R \to \infty$, obtained throughout our paper by letting $\tau \to \infty$ and keeping b fixed, the evolution of these plateaus is given by the CTDE:

$$x(t) = \frac{F(x(t-\tau))}{b} \equiv G(x(t-\tau)). \tag{3}$$

We note that time is still continuous in this difference equation. A further simplification of the dynamics in this singular limit results from discretizing time in units of one delay, and associating only one value of the state variable x with each time unit. The dynamics can then be cast in the form of a discrete-time map (see e.g. [7]):

$$x_{n+1} = \frac{F(x_n)}{b} = G(x_n). \tag{4}$$

Hence, for a constant initial function on $(-\tau, 0)$, the values of the successive plateaus are predicted by this map.

2.2. Spectral behavior

To further investigate the properties of high-dimensional solutions of such first-order DDEs, we calculate the spectral properties of solutions. We numerically generate a long solution time series starting with a constant initial

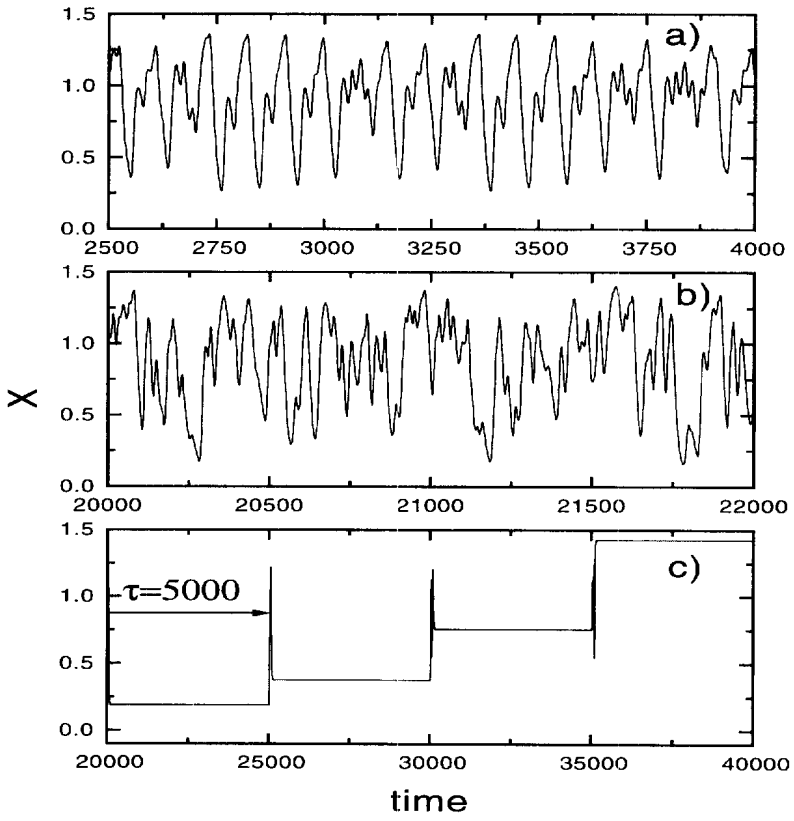

Fig. 1. Solutions of the Mackey–Glass equation, Eq. (2), for delay values of (a) $\tau = 25$, (b) $\tau = 200$, and (c) $\tau = 5000$. Other parameters are $a = 0.2$ and $b = 0.1$. A fixed step fourth-order Runge–Kutta method was used with integration time step 0.01. Linear interpolation was used for the required two midpoint evaluations of the delayed variable. The initial condition was a constant (0.8) on the delay interval $(-\tau, 0)$ in each case. The solution was found to be insensitive to the value of the constant initial condition (unless it is equal to 1, the unstable fixed point). Asymptotic solutions are shown in (a) and (b): the transients in (c) have not completely decayed; further this plateau solution is unstable.

condition on $(-\tau, 0)$. This solution is divided into many adjacent pieces. The power spectrum for each piece is computed using the Fast Fourier Transform – periodogram method; the individual results are finally averaged to produce an "averaged" power spectrum.

Fig. 2 shows power spectra from solutions of the Mackey–Glass equation for different delays using constant initial functions. We cannot exclude the possibility that different initial functions lead to different asymptotic chaotic solutions with different spectra and dynamical invariants, i.e. that the dynamics are multistable [12]. However, for a given delay, all constant initial functions tested yielded solutions having similar average power spectra.

When the delay is small (e.g. $\tau = 25$, as in Fig. 2(a)), the spectrum is broadband with a few broad peaks, a familiar characteristic of chaotic motion. There does not appear to be any clear relationship between the position of these few peaks and the frequency of the solutions obtained from a linearization of the dynamics around the fixed point (see Section 3).

However, if the delay is increased further to, e.g., $\tau = 200$ (Fig. 2(b)), a clear periodic modulation of the broadband background appears, as first noted in [2]. Further, the mean decay rate of this background no longer changes for larger delay values (the rate is the same in Figs. 2(b) and (c)), and is well-fitted over a large range by an exponential (Fig. 2(c)). The number of peaks in the power spectrum increases linearly with the delay, and for the accuracy used

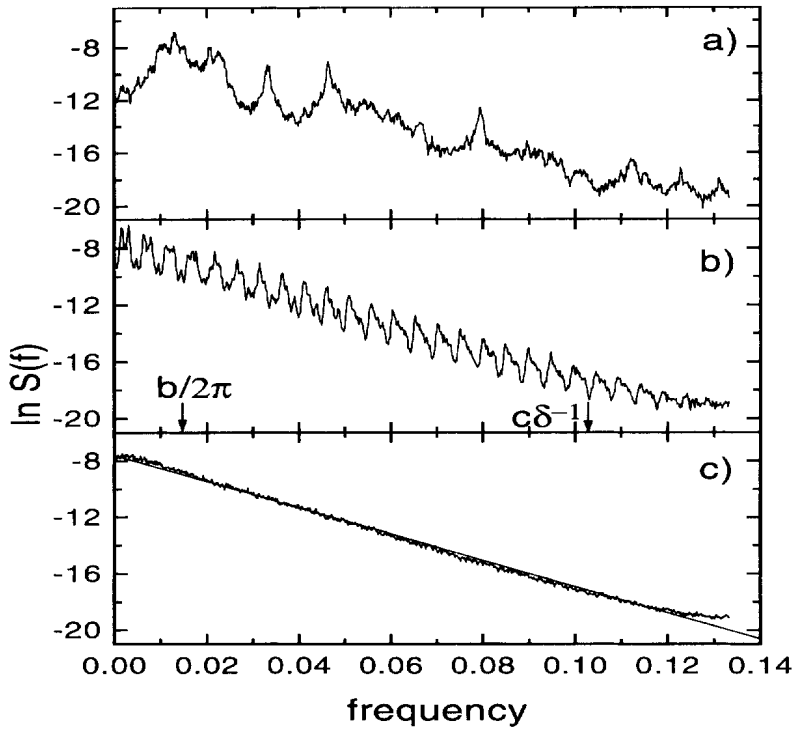

Fig. 2. Power spectra of solutions of Eq. (2) for the parameters used to generate the time series in Fig. 1; (a) $\tau = 25$, (b) $\tau = 200$, and (c) $\tau = 5000$. The spectra are obtained using the FFT algorithm, and are averages of spectra from 100 consecutive 8192-point time series. The integration time step is 0.01 s. The spectrum for $\tau = 5000$ is fitted to $y = C_1 + C_2 f$ with $C_1 = -7.6$ and $C_2 = -93.02$. The sampling time is 3.75 s. A Hanning window was used for all spectra in our study.

in our simulations, the modulation can no longer be seen when $\tau \geq 2000$, due to the finite frequency resolution in our spectra (see Fig. 2(c)). Let us assume that two peaks can be resolved if their centers are separated by at least $2\Delta_f$, where Δ_f is the width of one peak. Estimating the width of each peak as $\Delta_f = 0.00025$ Hz, we expect that neighboring peaks can be resolved if $\tau^{-1} \geq 2\Delta_f$, which agrees with our observation.

Fig. 3 shows a power spectrum for $\tau = 200$, as in Fig. 2(b), but using a smaller sampling time of 1 rather than 3.75 s (note that time in Eq. (2) is not dimensionless, and thus we choose an arbitrary time unit of 1 s throughout our work). We find that the modulation seen in Fig. 2(b) begins to die out past $c\delta^{-1}$, and disappears around $f = 0.14$ Hz. Here c is a system-dependent constant as discussed in Section 4.1, and δ is defined below. Also, the rate of decay seen in the range where the periodic modulation is present is the same as in Fig. 2(b). This suggests that aliasing effects, while potentially present because the solution is resampled with a time step larger than the integration time step, seem to slightly affect power estimates only at the very highest frequencies, i.e. those close to the Nyquist frequency used for the computation of a given spectrum. We have found behaviors with increasing delay similar to those in Figs. 2 and 3 for spectra of the Ikeda equation. For example, Fig. 4 shows a modulation as in Fig. 2(b) for a ratio of delay-to-response time of $R = 20$. However, we note a difference in line shape between the Mackey–Glass and Ikeda cases, the line shape being much simpler in the latter case. This difference will be explained in Section 5.

Our spectra for large delays can be decomposed into three different ranges of frequencies: (1) the low frequency range $0 < f < b/2\pi$, (2) the mid-to-high frequency range $b/2\pi \leq f \leq c\delta^{-1}$ (δ being the correlation time of the feedback term – see below, plus Figs. 2(b), 4–6), where the periodic modulation is clearly seen for large delays, and (3) the very high frequency range $f > c\delta^{-1}$; this latter range is shown only in Fig. 3. The spectral features

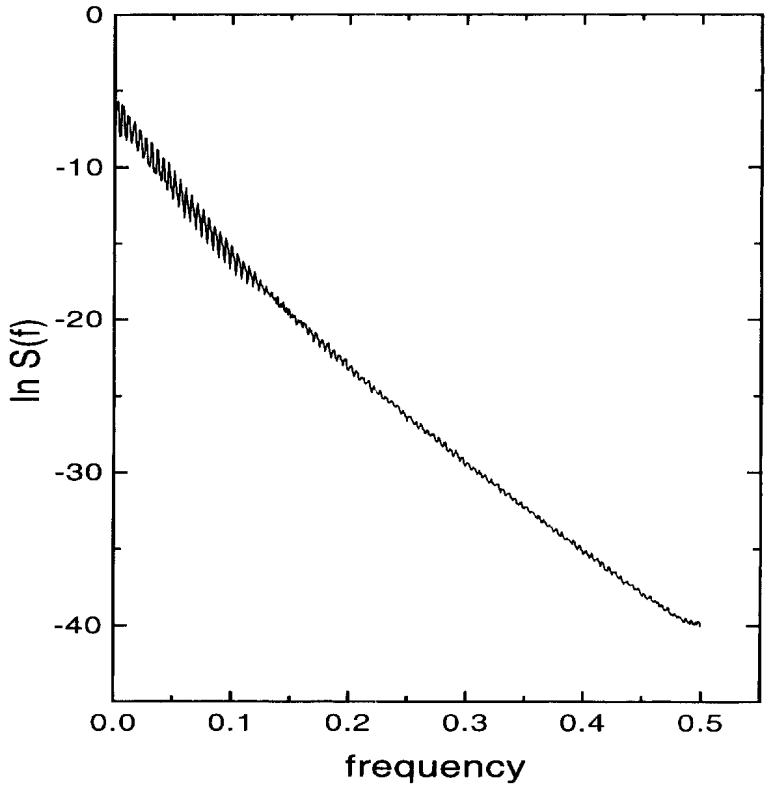

Fig. 3. Power spectrum for $\tau = 200$, as in Fig. 2(b), but with a sampling time of 1, i.e. a Nyquist frequency of 0.5 Hz. The spectrum in (0, 0.12) Hz was not changed (compare Fig. 2(b)) by using this smaller sampling time.

in region (1) can be understood by considering the delayed feedback in Eq. (2) as a forcing or "input" term in a non-autonomous system. By Fourier transforming Eq. (2), as in conventional linear systems analysis, we can write

$$j2\pi f X(f) = -bX(f) + \tilde{F}(f), \tag{5}$$

where $\tilde{F}(f)$ is the Fourier transform of the nonlinear feedback function. The magnitude squared amplitude (MSA) response function, relating the "output" $X(f)$ to the "input", is then:

$$|r(f)|^2 = \frac{|X(f)|^2}{|\tilde{F}(f)|^2} = \frac{1}{b^2 + 4\pi^2 f^2}. \tag{6}$$

We have verified numerically that the power spectrum of the output $x(t)$ and the input $F(x(t))$ for Eq. (2) are indeed related by Eq. (6) (not shown).

Fig. 4. The power spectrum of the Ikeda equation, i.e. Eq. (1) with $F(x(t-\tau)) = 2.1b^{-1}\pi \sin(x(t-\tau))$ with parameters $b = 1$ and $\tau = 20$. The spectrum is obtained from 100 consecutive 8192-point time series with an integration time step of 0.01 s and a sampling time of 0.16 s.

Fig. 5. Autocorrelation function of the feedback term $F(x(t-\tau))$ for the Mackey–Glass equation (Eq. (2)) in the chaotic regime ($a = 0.2, b = 0.1$) for various delays: (a) $\tau = 31.8$, (b) $\tau = 50$, (c) $\tau = 100$ and (d) $\tau = 200$. The correlation time δ, at which the autocorrelation decays to $1/e$ times its maximum value of 1 (at lag $s = 0$), is found to be 9.72 s in all cases.

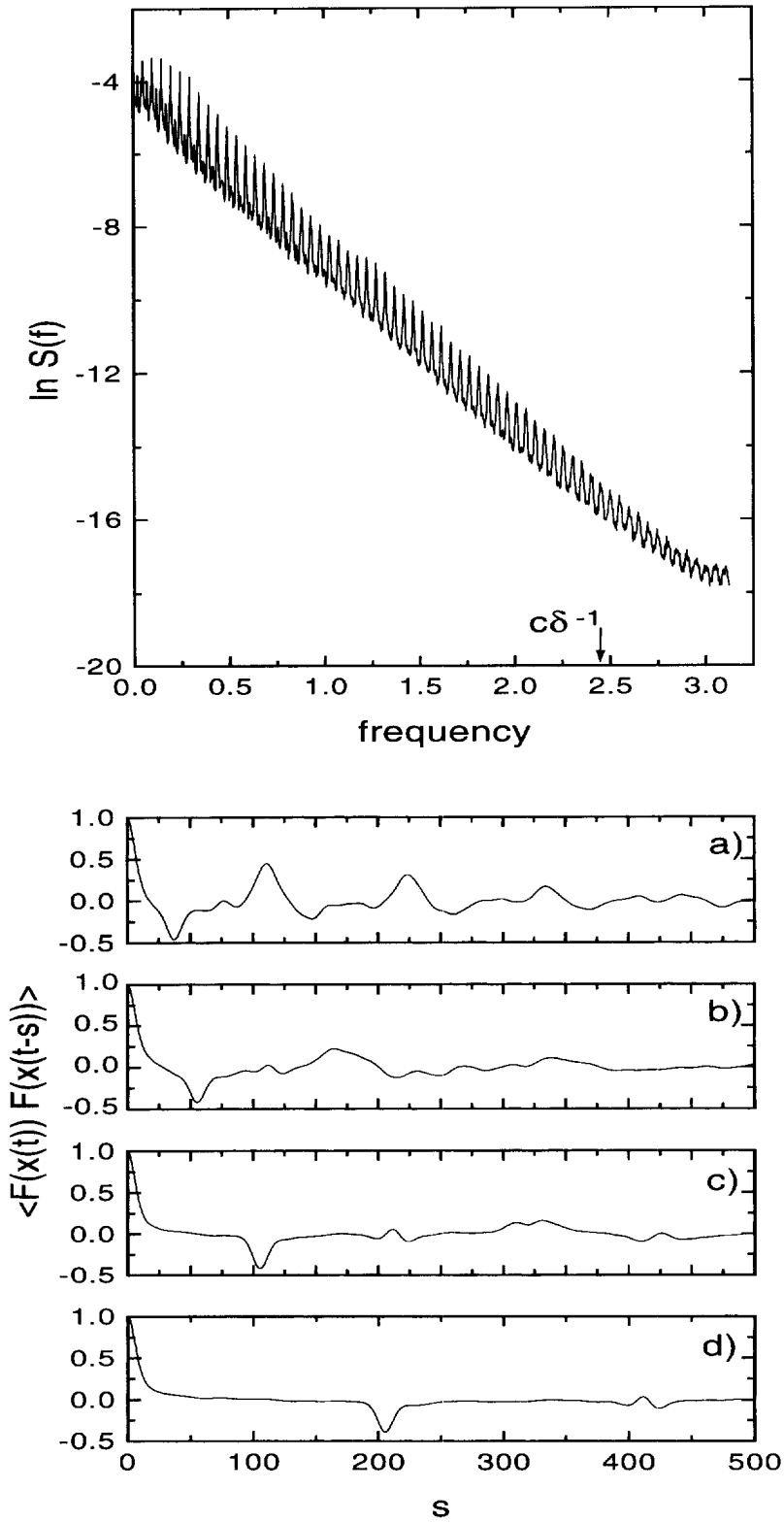
ln S(f)
-4
-8
-12
-16
-20
0.0
0.5
1.0
1.5
2.0
2.5
3.0
frequency
cδ -1
<F(x(t)) F(x(t-s))>
a)
b)
c)
d)
1.0
0.5
0.0
-0.5
0
100
200
300
400
500
s

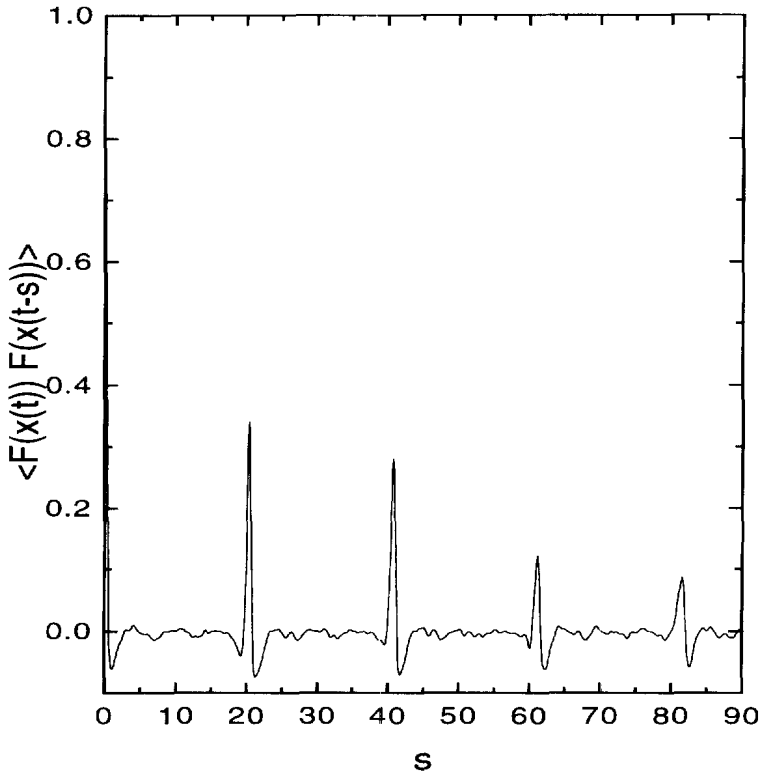

Fig. 6. Autocorrelation function of the feedback term for the Ikeda equation (see Fig. 4) with $\tau = 20$. The correlation time δ, at which the autocorrelation decays to $1/e$ times its maximum value, is found to be 0.35 s.

If $f \ll b/2\pi$, the MSA response function is $\approx 1/b^2$, so that in this leftmost part of region (1) fluctuations are amplified by $\approx 1/b^2$ from one delay interval to the next, in agreement with the difference equation (4) (see also [3]). As will be shown in Section 5, the shape of the peaks in this low-frequency region are similar to those for the CTDE (Eq. (3)) (Figs. 12 and 13), except that each main peak for the DDE is composed of two peaks rather than four in the CTDE, due to the limited resolution of our spectrum calculation for the DDE. The CTDE in fact can be used to relate the low-frequency spectral features of the DDE to those of the discrete-time map (Eq. (4)). As we move towards $b/2\pi$, the frequency dependence of the denominator in Eq. (6) comes into play, yielding a Lorentzian-type of decay which carries into the beginning of region (2). Region (1) can be assimilated with the "core range" in the terminology of Ikeda and Matsumoto [3], i.e. it contains the most dominant (i.e. most energetic) Fourier modes of the chaotic motion.

In region (2), the spectrum initially follows Eq. (6), but quickly gives way to an exponential decay over the remainder of this range. In fact, most of region (2) is well-fitted by

$$S(f) = Ae^{-\mu^{-1}f}, \tag{7}$$

where A is a constant and μ^{-1} is a spectral decay rate (in seconds: see Fig. 3). This region of exponential decay can be associated with the so-called dissipative range [3], characteristic of viscous dissipation at high frequency (or high wave number) in the context of turbulent flow. Region (3) is found to exhibit a slower decay, which is also to a good approximation exponential over a substantial part of its range ($0.2 < f < 0.4$ Hz).

For the Mackey–Glass equation, the integrated power S_I is found not to depend on the delay, provided this delay is larger than approximately 50, i.e. provided $R > 5$ (since $b = 0.1$). With negligible error, this integrated power can be approximated by

$$S_I = \int_0^{c\delta^{-1}} S(f)\,\mathrm{d}f = \frac{A}{\mu^{-1}}(1 - \mathrm{e}^{-\mu^{-1}c\delta^{-1}}) \simeq C(0), \tag{8}$$

where $C(0)$ is the autocorrelation function of $x(t)$ at zero lag (by the Wiener–Khintchine theorem, the integrated power in the spectrum is equal to $C(0)$). Thus, past a certain delay, the power in the signal $x(t)$ is constant, and consequently, the variance $C(0)$ of $x(t)$ becomes constant.

3. Linear stability analysis

We now show that the frequencies of the peaks that make up the modulated part of the power spectrum at large delays, such as for $\tau = 200$ in Fig. 2(b), agree very well with the frequencies of linear modes obtained by linear stability analysis of the DDE. These modes are determined by the characteristic equation of the DDE linearized around its fixed point x^* (which of course is unstable in the chaotic regime):

$$\frac{\mathrm{d}x(t)}{\mathrm{d}t} = -b(x(t) - x^*) + \beta(x(t-\tau) - x^*) + \cdots, \tag{9}$$

where $\beta = F'(x^*)$. If we take trial solutions of the form $u(t) = x(t) - x^* = u_0\mathrm{e}^{st}$, the characteristic equation becomes

$$s + b - \beta\mathrm{e}^{-s\tau} = 0. \tag{10}$$

Eq. (10) has an infinite number of roots $s_n = \lambda_n \pm \mathrm{i}2\pi f_n$, with f_n satisfying (see also [19])

$$\frac{(n-1/2)}{2\tau} < f_n < \frac{n}{2\tau}, \quad n = 1, 3, 5, \ldots \tag{11}$$

The mode associated with s_n goes unstable when λ_n becomes positive (in particular, the fixed point goes unstable when λ_1 becomes positive). If the delay is increased much beyond the response time b^{-1}, more and more modes cross the imaginary axis, thus becoming unstable with period close to $2\tau/n$. For delay increases, a mode that has gone unstable remains unstable.

All modes show up as clear peaks in the power spectrum at frequencies corresponding to those of the roots, with the most unstable ones being the dominant ones (Figs. 2 and 7). Some of the stable modes close to the imaginary axis appear also in the power spectrum because of nonlinear coupling to the unstable modes. In fact, due to nonlinearity, even the most unstable modes in the dissipative range appear in the power spectrum. It is as if all these eigenfrequencies are excited by the chaotic fluctuations, even though they are stable in the absence of these fluctuations. One can expect that the number of degrees of freedom in the system is directly related to these "spectrally visible" unstable and stable modes of the linearized system (see Section 4).

Hence, each peak of this modulation corresponds to a mode of oscillation predicted by linear stability analysis around the fixed point. This one-to-one correspondence between the peaks in the power spectrum and the linear modes has, to our knowledge, been studied only for periodic systems [20], as well as for low-dimensional chaos [21] when the delay is not too large compared to the response time. In this latter case, the correspondence is not very good because the modes do not appear at the same frequencies as the spectral peaks. It is also clear from our

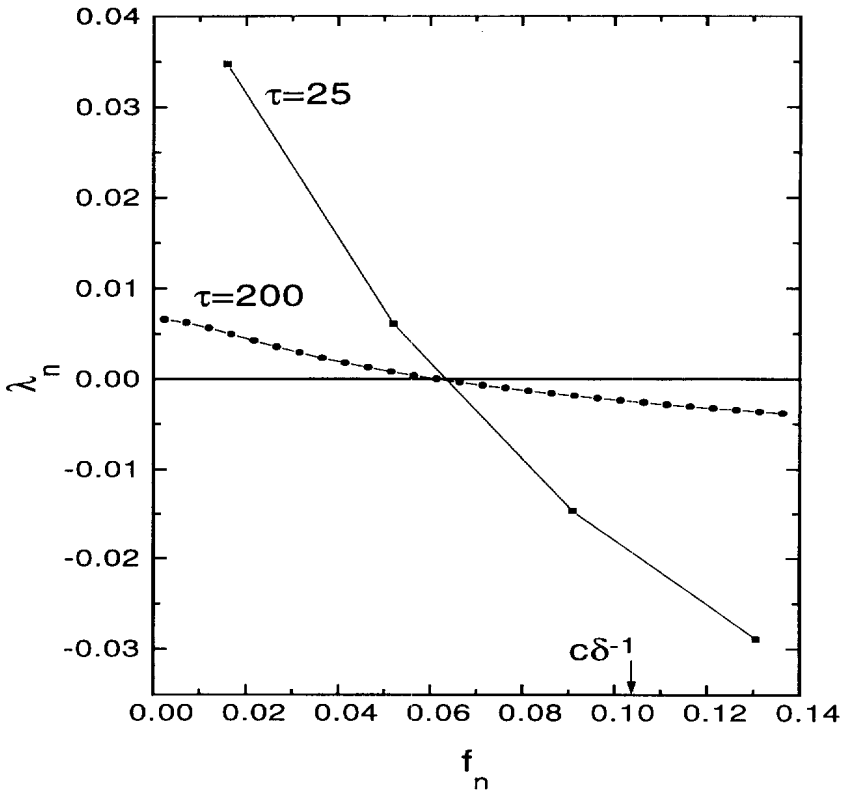

Fig. 7. Roots of the characteristic equation (Eq. (10)) obtained by linearizing the Mackey–Glass equation (Eq. (2)) around the fixed point. (a) $\tau = 25$; (b) $\tau = 200$. Note that the real part λ of the root (ordinate) is plotted against its imaginary part $\omega/(2\pi) = f$. Other parameters are $a = 0.2$, $b = 0.1$.

results that, at larger delays, most of the energy in the chaotic waveform lies at the low frequencies (the ordinate is logarithmic). This is similar to the case of fluid turbulence, where most of the energy lies in the long wavelength modes.

We also note that the real parts of the roots decrease with increasing delay (Fig. 7). This explains why the peaks in the power spectrum decrease in amplitude with increasing delay. At the same time, the peaks become closer, since their spacing is proportional to $1/\tau$, until they can no longer be resolved using a given level of frequency resolution in the spectral calculation. An approximate expression for the imaginary and real parts of these modes can be obtained for $\lambda_n \approx 0$:

$$f_n = \frac{n}{2\tau}\left(1 - \frac{1}{b\tau}\right) \approx \frac{n}{2\tau}, \quad n = 1, 3, 5, \ldots \tag{12}$$

and for n large, these modes decay as

$$\lambda_n = -\frac{1}{\tau}\ln\left(\frac{-2\pi f_n}{\beta}\right) \approx -\frac{1}{\tau}\ln n - \frac{1}{\tau}\ln\left(\frac{-\pi}{\beta\tau}\right). \tag{13}$$

This dependence of the real part of the eigenvalue on the logarithm of the root number has also been found for the Lyapunov exponents [2,3]. Ikeda and Matsumoto [3] further suggested (without showing it) that the Lyapunov exponents with larger negative values, for which this logarithmic scaling of exponents with exponent number is

seen, in fact correspond to the linear modes. The reason for this is that the decay rates (as a function of n) of the real part of the roots and of the Lyapunov exponents are the same when n becomes large. Thus, these negative Lyapunov exponents can be estimated from the expression for the stable modes (Eq. (13)), i.e.

$$\lambda^{L}_{(n+1)/2} \approx \lambda_n, \tag{14}$$

for n odd and sufficiently large. Comparing the Lyapunov exponents recently computed by Sigeti [16] with our roots of the characteristic equation, we find that the Lyapunov exponents indeed agree with the real parts for sufficiently large n. For example, for $\tau = 200$ in the Mackey–Glass equation, we find the following real parts λ_n and Lyapunov exponents λ^{L}_i (remember only odd numbered modes are seen in the spectrum): ($\lambda_{29} = -0.000695$, $\lambda^{\mathrm{L}}_{15} = -0.00075$), ($\lambda_{31} = -0.00102$, $\lambda^{\mathrm{L}}_{16} = -0.00102$), ($\lambda_{33} = -0.00132$, $\lambda^{\mathrm{L}}_{17} = -0.00132$), ($\lambda_{35} = -0.00161$, $\lambda^{\mathrm{L}}_{18} = -0.00162$), ($\lambda_{37} = -0.00188$, $\lambda^{\mathrm{L}}_{19} = -0.00193$), ($\lambda_{39} = -0.00214$, $\lambda^{\mathrm{L}}_{20} = -0.00222$), ($\lambda_{41} = -0.00238$, $\lambda^{\mathrm{L}}_{21} = -0.00250$).

These negative modes do not, a priori, provide information on attractor dimension (such as the Lyapunov dimension) and Kolmogorov–Sinai entropy, since one needs the positive exponents and the first few negative ones to estimate such quantities [22,23]. Nevertheless, this agreement between modes and exponents shows that apparently nonlinear characteristics of DDEs, such as self-oscillation frequencies and negative Lyapunov exponents, are in fact closely related to simple linear characteristics. In the next section, we discuss how other linear properties of the DDE are related to dynamical invariants such as dimension and Lyapunov exponent spectrum.

4. Dynamical invariants from power spectra

4.1. Estimating the dimension

For the Mackey–Glass equation, the information dimension d of the motion on the attractor has been shown to increase linearly with the delay [2,5]. The same applies to the Lyapunov dimension, since both dimensions were shown to be equal [2]. The proportionality constant between delay and dimension is closely governed by the autocorrelation time δ of the feedback $F(x(t))$ ([5]: see Figs. 5 and 6). This time can be estimated as the $1/e$ decay time of the central peak in the autocorrelation function from its maximal value at zero lag, i.e. at $s = 0$ (the other symmetric half of this peak is at negative lags, which are not shown). A good estimate of the Lyapunov dimension is then $d = c\tau/\delta$, where c is a constant that depends on the particular feedback used. For example, in the Mackey–Glass equation c is close to one [2,5]; for Ikeda equation, $c \approx 0.85$ [5].

We have found that d can be estimated from either the power spectrum or linear stability analysis. Since power spectra can be easily calculated with standard algorithms, and linear stability analysis is straightforward to carry out, estimating dimension in these ways clearly is advantageous in comparison with algorithms to compute, e.g. the correlation integral or the spectrum of Lyapunov exponents. In particular these latter methods, while standard tools, are particularly time consuming for high-dimensional systems such as those of interest in our study.

Our estimation method works as follows. From the spectral point of view, the attractor dimension can be estimated as the number of peaks within the frequency range $(0, c\delta^{-1})$. Since each peak corresponds to a mode, the dimension also represents the number of roots of the characteristic equation (Eq. (10)) within that range; this is the basis of the linear analysis estimate. For example, in the Mackey–Glass model with parameters (see [2]) $a = 0.2$, $b = 0.1$, and a delay $\tau = 200$, we found $\delta \simeq 9.72$ (see Fig. 5) and a dimension $d = c\tau/\delta \simeq 21$ (see Table 1). The number of peaks in the power spectrum within the $(0, c\delta^{-1})$ frequency range is also found to be approximately 21, in good agreement with the Lyapunov dimension found in [2]. For the Ikeda model, the Lyapunov dimension found for the parameters $\tau = 20$ and $\tilde{\mu} = 2.1$ is $\simeq 42$ [6]. We compute $\delta = 0.35$ (see Fig. 6), which yields a dimension

Table 1
Numerical results at different delays for the Mackey–Glass equation

τ	d_S	d_{KY}	$\sum\lambda_L^+$	$\sum\lambda_n^-$	μ	$\mu/\sum\lambda_L^+$	$\mu/\sum\lambda_n^+$
50	6	5.37	8.99×10^{-3}	4.067×10^{-2}	1.075×10^{-2}	1.196	0.264
100	11	10.34	1.022×10^{-2}	4.062×10^{-2}	1.075×10^{-2}	1.052	0.265
200	21	20.28	1.041×10^{-2}	4.063×10^{-2}	1.075×10^{-2}	1.033	0.265

d_S is the dimension of the attractor estimated from the power spectrum by counting the number of peaks within the range $(0, c\delta^{-1} = 0.103)$ Hz (Fig. 5), where $c = 1$. This dimension is equal to the number of Lyapunov exponents and is approximately given by τ/δ. d_{KY} is the Kaplan–York dimension. λ_L^+ are the positive Lyapunov exponents. λ_n^+ are the real parts of solutions of the characteristic equation of the linearized system (Eq. (10)). μ is the exponential decay constant of the power spectrum $S(f) = Ae^{-\mu^{-1}f}$, where A is a constant.

$d = c\tau/\delta = 48$ (where $c \approx 0.85$ [5]), which is close to 42. Further, estimating dimension by counting the number of spectral peaks in the corrected range $(0, c\delta^{-1})$, as the results in [5] would suggest, yields approximalety 48 (see Fig. 4), and thus there is agreement with the value obtained above.

We note that the spectra show a continuous variation of features as the delay increases: while the background converges to a constant mean slope, the number of modes increases smoothly and their amplitude decreases, following the behavior of the linear modes (more cross the imaginary axis and asymptotically their real parts decrease); consequently, the fundamental frequency (roughly $1/2\tau$ as predicted by Eq. (12)) steadily decreases. Given the relationship found between the number of modes within the characteristic bandwidth $(0, c\delta^{-1})$ and the Lyapunov dimension, it is reasonable to assume that the attractor dimension also increases smoothly with the delay for high delays. As Farmer [2] found that dimension still increases in small jumps at high delays, more work is perhaps needed to verify whether these jumps really occur and what their origin is.

4.2. *Lyapunov exponents and power spectrum decay*

For the ring-cavity laser, the Lyapunov dimension increases linearly with the delay, but the metric entropy stays constant past a certain delay value [4]. The fact that the metric entropy saturates but the dimension keeps increasing with delay implies that the Lyapunov exponents scale as $1/\tau$, as has been pointed out in various studies (see e.g. [2,4]). The findings of Section 3 support this dependence. Indeed, we found that the negative Lyapunov exponents are closely given by the real part of the roots of the linear characteristic equation. As shown in Eq. (13), these real parts also scale as $1/\tau$.

Table 1 presents our attractor dimension estimates d_S based on the power spectrum. These values agree with estimates based on the Kaplan–Yorke conjecture d_{KY} using the Lyapunov exponent estimates in [16] (as well as other sources). The sum of positive Lyapunov exponents $\sum\lambda_L^+$ converges to a constant when the delay is increased, and can be related to the decay rate of the power spectrum μ^{-1} in the dissipative range as follows:

$$\mu \approx \sum\lambda_L^+. \tag{15}$$

This result is significant since the chaotic fluctuations of longer wavelengths are related to the positive Lyapunov exponents in that range. In region (3) beyond the dissipative range, the Lyapunov exponents are very negative, and therefore it is less likely that the decay rate in this range is governed by the positive Lyapunov exponents. We found that this decay rate μ^{-1} can also be related to the sum of the unstable linear modes by

$$\mu \approx \sum\lambda_n^+/4. \tag{16}$$

Hence, the relation between the positive Lyapunov exponents and the unstable linear modes is

$$\sum\lambda_L^- \approx \sum\lambda_n^+/4. \tag{17}$$

This correspondence established using the decay rate in region (2) may be a peculiarity of the Mackey–Glass and Ikeda systems, i.e. of first-order DDEs with feedback dynamics; for other lower-dimensional ODEs, a correspondence can perhaps only be found at high frequency, as the results in [16] suggest. It is the modulation in the spectrum at mid-frequencies and large delays ($\tau > 100$) which initially drew our attention to a possible matching of the sum of Lyapunov exponents with the spectral decay rate in the region (2) containing much of the energy in the signal. This is the region where the modulation is present, i.e. where most of the dominant modes are fluctuating.

4.3. Distributed delays

To obtain more insight into the exponential behavior of DDE spectra, we now study the more realistic case of "distributed delays" [24,25] rather than of single fixed delays. In this distributed delay case, the system state in the present is affected by not one, but many past state values via a memory kernel $K(t)$:

$$\frac{\mathrm{d}x}{\mathrm{d}t} = f(x(t), z(t)), \quad z(t) = \int_{-\infty}^{t} K(t-u)x(u)\,\mathrm{d}u. \tag{18}$$

By choosing a gamma distribution kernel

$$G_\alpha^m(q) = \frac{\alpha^{m+1}}{m!} q^m \mathrm{e}^{-\alpha q}, \quad \alpha, m \geq 0, \tag{19}$$

the DDE can be transformed to a finite number of ODEs

$$\frac{\mathrm{d}y_0}{\mathrm{d}t} = f(y_0, y_{m+1}), \qquad \frac{\mathrm{d}y_i}{\mathrm{d}t} = \alpha(y_{i-1} - y_i), \quad i = 1, 2, \ldots, m+1. \tag{20}$$

In the limit $(m, \alpha) \to \infty$ (keeping their ratio constant), the kernel becomes a delta-function, and this set of ODEs approaches formally the DDE, with the average delay given by

$$\overline{\tau} = \frac{\int_0^\infty q G_\alpha^m(q)\,\mathrm{d}q}{\int_0^\infty G_\alpha^m(q)\,\mathrm{d}q} = \frac{m+1}{\alpha}. \tag{21}$$

Fig. 8 shows three spectra obtained for three different values of m, adjusting α in order to have an average delay of $\overline{\tau} = 200$ in each case. For $\overline{\tau} = 200$ when $m = 199$ ($\alpha = 1$), the power spectrum starts to exhibit the peak structure at low frequencies, as seen in Fig. 2(b), even though the decay rate of the exponential background is steeper than for the DDE. For increasing m, the slope approaches that for the DDE; as $(m, \alpha) \to \infty$, the power spectra likely converges to that for the DDE.

The frequencies of the modes are the roots of (Eq. (20)) around the fixed point:

$$(s+b)(s+\alpha)^{m+1} - F'(x^*)\alpha^{m+1} = 0. \tag{22}$$

This equation has $m+2$ roots corresponding to $m+2$ frequencies. To study the limit of Eq. (22), we write it in the following form

$$(s+b)\left(1 + \frac{s}{\alpha}\right)^{\alpha\overline{\tau}} - F'(x^*) = 0. \tag{23}$$

In the limit $\alpha \to \infty$, the term $(1 + s/\alpha)^{\alpha\overline{\tau}}$ goes to $\mathrm{e}^{s\overline{\tau}}$, and the characteristic equation of the distributed delay system becomes identical to that for a DDE with fixed delay $\overline{\tau}$:

$$s + b - F'(x^*)\mathrm{e}^{-s\overline{\tau}} = 0. \tag{24}$$

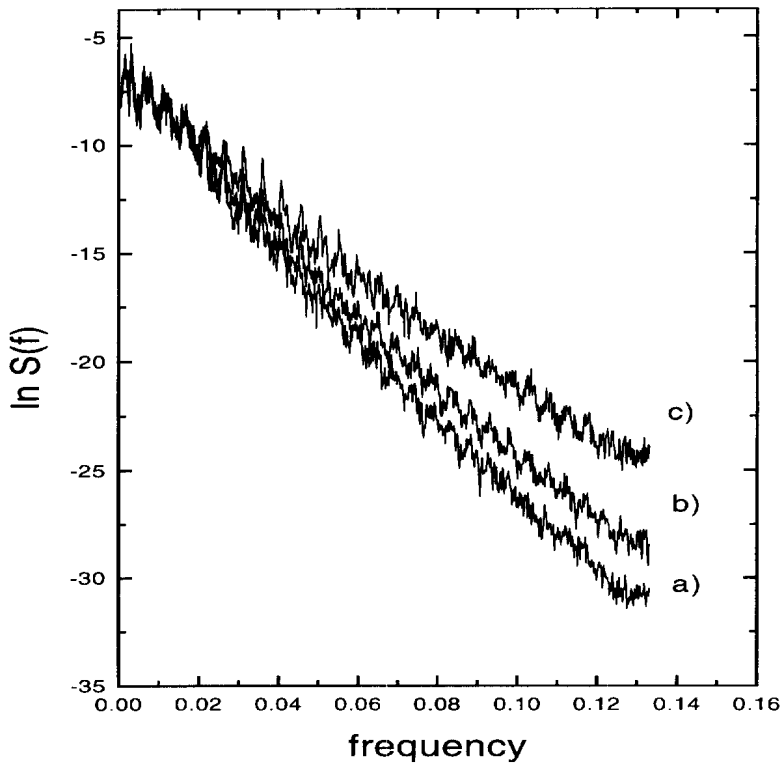

Fig. 8. The power spectrum of the distributed delay approximation, Eq. (20), to the Mackey–Glass equation, Eq. (2), with an average delay $\bar{\tau} = (m + 1)/\alpha = 200$. The parameters for the Gamma memory kernel are: (a) $m = 199$ and $\alpha = 1$, (b) $m = 399$ and $\alpha = 2$, and (c) $m = 799$ and $\alpha = 4$. The spectrum converges to that in Fig. 2(b) as m in Eq. (20) is increased, i.e. as the approximation to the DDE improves. The peaks, which are most prominent in (c), correspond to the frequencies of the modes obtained from linear stability analysis around the fixed point of the system of ODEs, Eq. (22). These peaks are equivalent to those obtained with the DDE for $\tau = 200$. The sampling time is 3.75.

It is thus possible, for large m, to draw a correspondence between the center frequency of the spectral peaks with the roots of the characteristic equation, as we did for the DDE. We further conjecture that the number of peaks in the power spectrum can be used to estimate attractor dimension, and the spectrum decay to estimate the Kolmogorov entropy, as for the DDE.

5. CTDE solution spectra for piecewise constant initial functions

The solutions of the CTDE are chaotic; thus solutions for constant initial functions are unstable, i.e. small perturbations to neighboring points on a plateau will diverge exponentially in time. Nevertheless, we have found that the spectra of such CTDE solutions can be used to estimate attractor dimension for DDEs, and further suggest an origin for the peak shapes in DDE spectra at large delay ($\tau \approx 200$). This section investigates such CTDE spectra.

5.1. Power spectrum of solutions

In the limit ($R \to \infty$), the solution of the DDE approaches the CTDE (Eq. (3)), and clear plateaus are observed if one takes piecewise initial functions (see Fig. 9). Their values are predicted by the map (4). In this case, the power

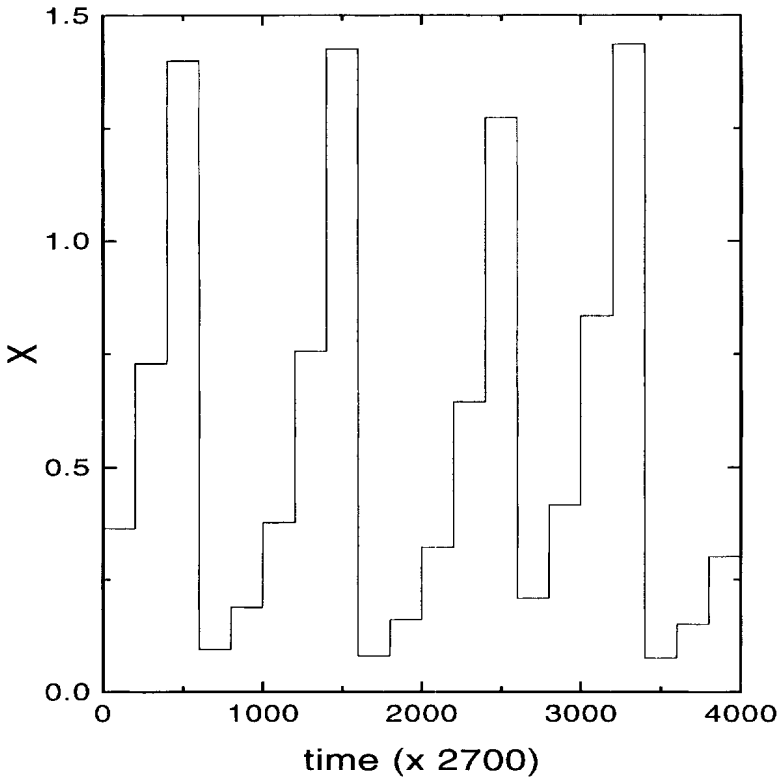

Fig. 9. Solution of the Mackey–Glass equation, Eq. (2), at very large delay $\tau = 540\,000$. Other parameters are $a = 0.2$, $b = 0.1$. This solution is equivalent to the one obtained with the continuous-time difference equation, Eq. (3). The integration time step is 2.7.

spectrum can be calculated analytically using the Fourier transform of a non-periodic signal with an infinite period ($T \to \infty$) as follows:

$$X(f) = \lim_{T\to\infty} \frac{1}{T} \int_0^T x(t) e^{2\pi i f t}\, dt. \tag{25}$$

We choose $T = N\tau$ (an integer multiple of the delay) with $N \to \infty$. Eq. (25) becomes

$$X(f) = \lim_{N\to\infty} \frac{1}{N\tau} \int_0^{N\tau} x(t) e^{2\pi i f t}\, dt. \tag{26}$$

For a constant initial function, the solution $x(t)$ is composed of plateaus of length τ, i.e. $x(t) = a_j$ for $j\tau < t < (j+1)\tau$, where $j = 0, 1, 2, \ldots (N-1)$, and the a_j's are constants. The above equation becomes

$$X(f) = \lim_{N\to\infty} \frac{1}{N\tau} \sum_{j=0}^{N-1} a_j \int_{j\tau}^{(j+1)\tau} e^{2\pi i f t}\, dt = \lim_{N\to\infty} \frac{e^{\pi i f \tau}}{\tau} \frac{\sin(\pi f \tau)}{\pi f} X_1(f), \tag{27}$$

where $X_1(f)$ is the Fourier transform of a series of points generated by the map (Eq. (4)). Using the transformation $f \to f\tau$ and the approximation $f/\tau \simeq \sin(f/\tau)$ at large delays, the power spectrum can then be

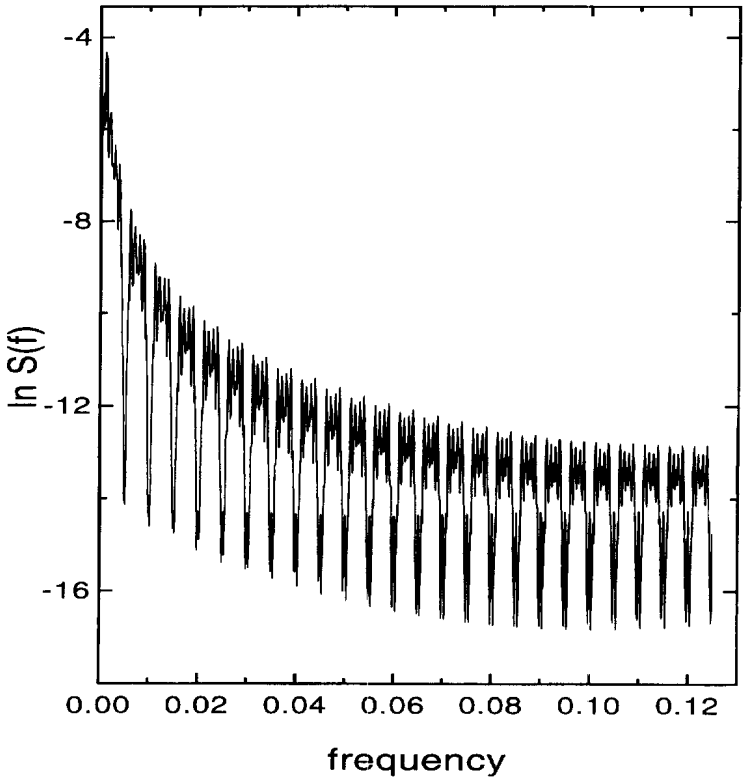

Fig. 10. Power spectrum of the Mackey–Glass equation (Eq. (2)) at very large delay $\tau = 540\,000$, for which the solutions are as shown in Fig. 9. The initial condition was constant. The integration time step is 2.7. The spectrum is similar to the one obtained with the CTDE in Fig. 13, even though the delay here is finite.

written as

$$S(f) = |X(f)|^2 = \frac{1}{\tau^2}\frac{\sin^2(\pi f)}{\sin^2(\pi f/\tau)} S_1(f), \tag{28}$$

where $S_1(f) = |X_1(f)|^2$ is the power spectrum of the map (Eq. (4)). Below, we will show that a similar form can be obtained for the power spectrum using the discretization of the time in units of τ in Eq. (3). Fig. 10 shows the power spectrum of the DDE at very large delay ($\tau = 540\,000$) which is equivalent to the power spectrum of the CTDE in Fig. 13.

5.2. *The spectrum of M parallel maps*

We now show how the discrete-time map, Eq. (4), can explain the shape of the spectral peaks for the DDE at finite delay, and also be used to estimate attractor dimension. This method is even easier and faster than that in Section 4, since it does not require a numerical integration algorithm (such an algorithm, along with an autocorrelation function estimator, are required, however, to obtain the correlation time δ). By discretizing the time delay τ in Eq. (3) into M points, the CTDE is equivalent to M difference equations (or M mappings in parallel), as shown in Fig. 11. We show below that the power spectrum of these M moving points is related to the power spectrum of the map (Eq. (4))

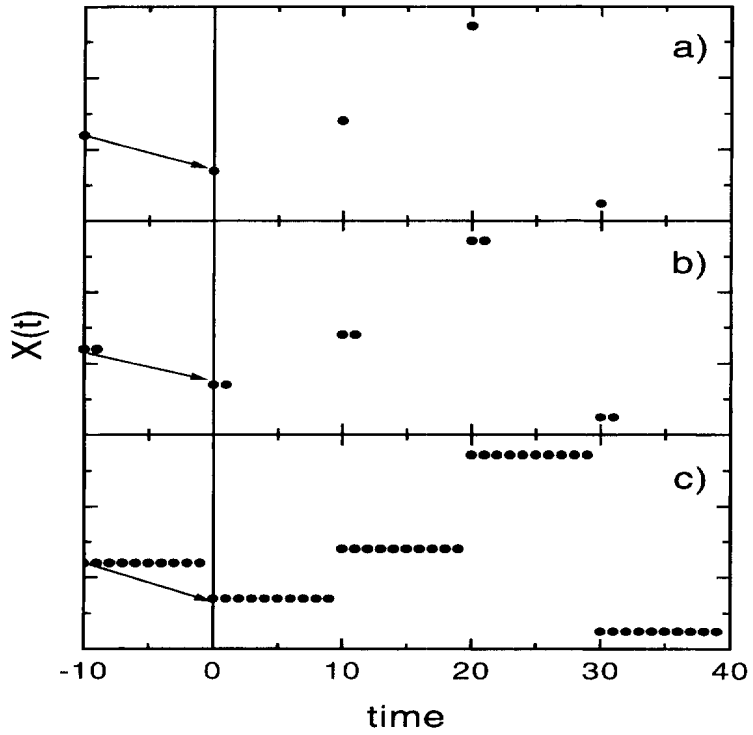

Fig. 11. Transition from a map evolving in discrete time to M maps evolving in parallel in discrete time. The points on $(-\tau, 0)$ evolve independently from one interval to the next, and so are mapped in parallel according to the map $x(i) = G(x(i-1))$. As M goes to infinity, the system of parallel maps becomes equivalent to the continuous-time difference equation, Eq. (3).

via a lowpass filter response function. In the following, we will consider the CTDE as M parallel ("decimated" is perhaps a better term) series of N points, each series of N points being generated by the map in Eq. (4). Each series $x_m(t)$, $m = 1, 2, \ldots, M$, can be represented as

$$x_m(t) = \sum_{j=0}^{N-1} G^j(x_{0m})\delta[t - (j-1)M\Delta - (m-1)\Delta], \tag{29}$$

where Δ is the sampling time and δ is the Dirac delta function. The series of $N * M$ points for the M moving points is given by

$$x(t) = \sum_{m=1}^{M} x_m(t). \tag{30}$$

The Fourier transform of these M parallel series is given by

$$\begin{aligned} X(f) &= \frac{1}{N * M} \int_{-\infty}^{+\infty} x(t) e^{2\pi i f t}\, dt \\ &= \frac{e^{-2\pi i f M\Delta}}{N * M} \sum_{m=1}^{M} e^{2\pi i (m-1) f \Delta} \sum_{j=0}^{N-1} G^j(x_{0m}) e^{2\pi i j f M\Delta}. \end{aligned} \tag{31}$$

Since $x(t)$ is discrete in time with time step Δ, its Fourier transform will be discrete in the frequency domain with frequency step $f_k = k/(M * N * \Delta)$, $k = 0, \ldots, (NM - 1)$. Eq. (31) becomes

$$X(f_k) = \frac{e^{-2\pi ik/N}}{N * M} \sum_{m=1}^{M} e^{2\pi i(m-1)k/(M*N)} \sum_{j=0}^{N-1} G^j(x_{0m}) e^{2\pi ijk/N}$$

$$= \frac{e^{-2\pi ik/N}}{M} \sum_{m=1}^{M} e^{2\pi i(m-1)k/(M*N)} X_m(f_k), \tag{32}$$

where

$$X_m(f_k) = \sum_{j=0}^{N-1} G^j(x_{0m}) e^{2\pi ijk/N}, \tag{33}$$

is the Fourier transform of the mth series of N points.

In the context of information storage in DDEs [13–15], the initial conditions of interest are piecewise constant functions on the interval $(-\tau, 0)$. This fact, along with the eventual goal of generalizing our results to arbitrary initial functions, lead us to pursue our calculation with initial functions made up of L constant plateaus in the interval $[-M\Delta, 0]$. We can then write for the Fourier transform of $N * M$ points from M parallel time series of N points:

$$X(f_k) = \frac{e^{-2\pi ik/N}}{M} \sum_{l=1}^{L} \sum_{m=(l-1)M/L+1}^{lM/L} e^{2\pi i(m-1)k/(M*N)} X_l(f_k)$$

$$= \frac{e^{-2\pi ik/N}}{M} \sum_{l=1}^{L} e^{2\pi i(l-1)k/(L*N)} \sum_{m'=1}^{M/L} e^{2\pi i(m'-1)k/(M*N)} X_l(f_k)$$

$$= \frac{e^{-2\pi ik/N}}{M} \sum_{m'=1}^{M/L} e^{2\pi i(m'-1)k/(M*N)} \sum_{l=1}^{L} e^{2\pi i(l-1)k/(L*N)} X_l(f_k). \tag{34}$$

This assumes that all chosen initial values for the plateaus belong to the attractor of the map; in other words, each plateau evolves in an asymptotic regime, once the transients have died out. If the map is ergodic, we can expect identical power spectra for time series starting from typical initial conditions. Therefore we can expect that, for any l,

$$|X_l(f_k)|^2 = |X_1(f_k)|^2. \tag{35}$$

Here $X_1(f_k)$ is the Fourier transform of the map (Eq. (4)). If the map has periodic solutions, then there is a finite number of attractor solutions, and each one can be obtained from any other one by a simple time shift. In this case, we can write

$$X_l(f_k) = X_1(f_k) e^{2\pi i\Psi_l}, \tag{36}$$

where $\Psi_l = \varphi_l - \varphi_1$ is the phase difference between $X_l(f_k)$ and $X_1(f_k)$. If the map is chaotic, the Fourier transforms will differ in phase at each frequency, but not in modulus since the spectra will be similar. In this case, one expects a more complicated relationship of the form $\Psi_l(k) = \varphi_l(k) - \varphi_1(k)$ where we have highlighted the frequency dependence. Hence we have the following general form for the Fourier transform of a CTDE solution with initial functions defined using L subintervals:

$$X(f_k) = \frac{e^{-2\pi ik/N}}{M} X_1(f_k) \sum_{m'=1}^{M/L} e^{2\pi i(m'-1)k/(M*N)} \sum_{l=1}^{L} e^{2\pi i|(l-1)k/(L*N)+\Psi_l(k)|}. \tag{37}$$

The power spectrum is

$$S(f_k) = |X(f_k)|^2 = |H(k)|^2 S_1(f_k), \tag{38}$$

where $S_1(f_k) = |X_1(f_k)|^2$ is the power spectrum of the map (Eq. (4)), $|H(k)|^2$ is the magnitude squared amplitude response

$$|H(k)|^2 = \frac{1}{M} \frac{\sin^2(\pi k/(L*N))}{\sin^2(\pi k/(M*N))} |Z(k)|^2 \tag{39}$$

with

$$Z(k) = \sum_{l=1}^{L} e^{2\pi i[(l-1)k/(L*N)+\Psi_l(k)]}. \tag{40}$$

This spectrum $S(f_k)$ can be estimated using the periodogram for $N*M$ points generated by the M parallel maps (Fig. 11). This periodogram is defined at $(N*M/2+1)$ frequencies as

$$\begin{aligned} S(0) &= |X(0)|^2, \\ S(f_k) &= \frac{1}{2}[|X(f_k)|^2 + |X(f_{N*M-k})|^2], \quad k = 1, 2, \ldots, \left(\frac{N*M}{2} - 1\right), \\ S(f_{N*M/2}) &= |X(f_{N*M/2})|^2. \end{aligned} \tag{41}$$

For M maps in parallel, f_k is defined for the following frequencies:

$$f_k = \frac{k}{M*N*\Delta} = 2f_c \frac{k}{M*N}, \quad k = 0, 1, \ldots, \frac{N*M}{2}, \tag{42}$$

where $f_c = 1/2\Delta$ is the Nyquist frequency.

5.3. The case of constant initial conditions

If $\Psi_l = 0, l = 1, 2, \ldots, L$ (same initial conditions), then

$$|Z(k)|^2 = \frac{\sin^2(\pi k/N)}{\sin^2(\pi k/(L*N))}. \tag{43}$$

The power spectrum takes the form

$$S(f_k) = \frac{1}{M^2} \frac{\sin^2(\pi k/N)}{\sin^2(\pi k/(M*N))} S_1(f_k), \tag{44}$$

with zeros at $k = N, 2N, \ldots, M*N/2$. This form is equivalent to the one found in Section 6.1 (see Eq. (28)) by replacing M with τ. Note that the maximum value of the denominator is 1, and that for low frequencies it decreases as $1/k^2$, i.e. as $1/f^2$. Figs. 12 and 14 show parallel map power spectra for, respectively, the Mackey–Glass and Ikeda models for $M = 1$, $M = 2$, and $M = 10$. We note that, for illustration purposes, we have normalized our spectra in order to keep the Nyquist frequency at 0.5. In fact, if we were to compare actual spectra for, e.g. $M = 1$

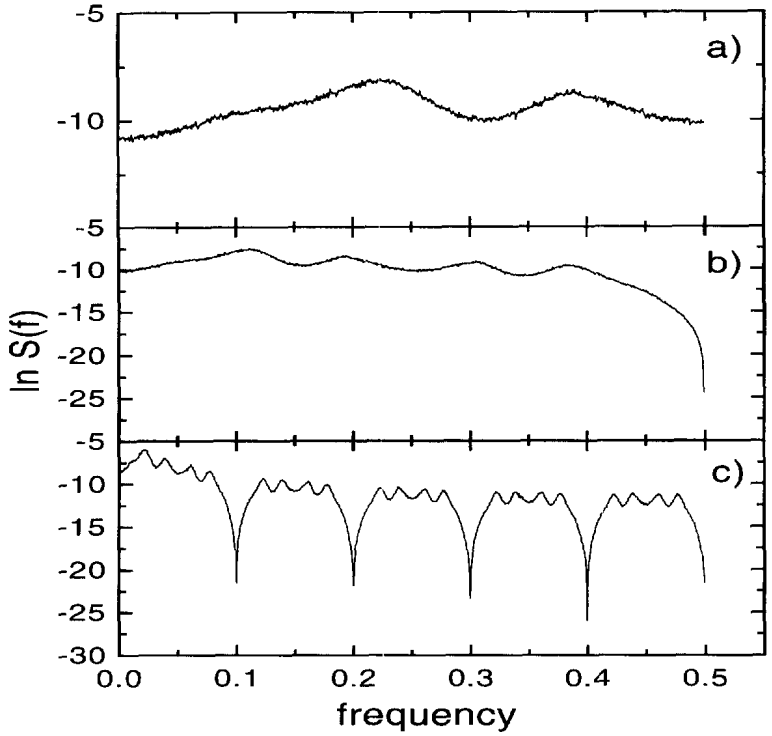

Fig. 12. Power spectra of the Mackey–Glass continuous time difference equation (CTDE), Eq. (3), $\dot{x}(t) = G(x(t-\tau))$ (see Fig. 11): (a) power spectrum of a single point evolving in time ($M = 1$); (b) same as is (a) but for $M = 2$ points on the delay interval evolving in time; (c) same as in (a) but for $M = 10$ points. The initial values for all points is the same in each case.

and $M = 10$, we would find that the spectrum for $M = 10$ extends over 10 times the frequency range of that for $M = 1$.

As M increases, more and more peaks are seen in the power spectrum. In fact, closer inspection reveals that the power estimates for higher frequency values for $M = 2$ are obtained by juxtaposing the spectrum for a single map (Figs. 12(a) and 14(a)) with its mirror image about the y-axis. This juxtaposition is then multiplied by the frequency-dependent filtering or "scaling" factor in Eq. (44), i.e. the prefactor of $S_1(f_k)$ on the right-hand side. Spectral estimates at higher values of M are similarly obtained by reflection, translation and scaling.

The filtering function $|H(k)|^2$ in Eq. (44) (see also Eq. (38)) affects the amplitude of the power and determines its zeros as well. The symmetries of the spectra can be seen to originate from the properties of the spectrum of M parallel maps without this filtering function. The spectral estimates over different frequency ranges are then related to each other by:

$$S(f_k) = S(f_{k+q*N}), \quad q = 1, \ldots, M-1; \quad k = 0, \ldots, N. \tag{45}$$

With the filtering function in place, the following translation and reflection relationships hold:

$$\begin{aligned} S(f_{k+(q-1)N}) &= |H(k+(q-1)N)|^2 S_1(f_k), \\ S(f_{k+(q-1/2)N}) &= |H(k+(q-1/2)N)|^2 S_1(f_{N/2-k}), \quad q = 1, \ldots, M/2; \quad k = 0, \ldots, N/2. \end{aligned} \tag{46}$$

Thus, one can construct piece by piece the whole power spectrum for M parallel maps.

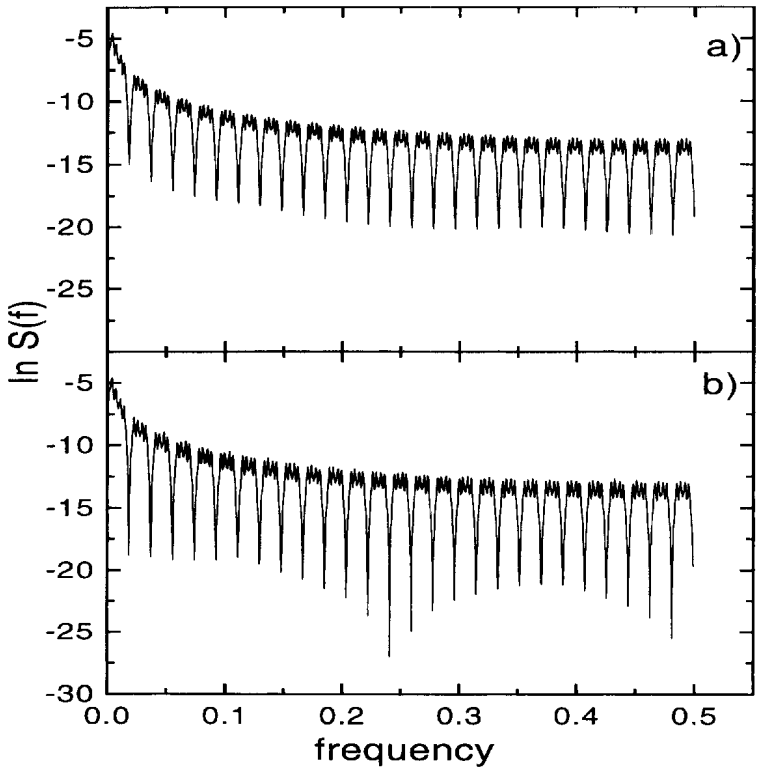

Fig. 13. Power spectra of the Mackey–Glass CTDE, Eq. (3), for $M = 54$ points on a delay interval evolving in parallel forward in time, calculated (a) from the time series generated by the CTDE, and (b) analytically using Eq. (44) in which $S_1(f_k)$ is the power spectrum computed numerically from the evolution of a single point ($M = 1$) following the map Eq. (4) (shown in Fig. 12(a)). The spectra are equivalent when the number of points used to calculate the FFT in (b) is equal to M times the number of points in (a). If the number of points used to calculate the FFT is the same in (a) and (b), then we have to multiply the power spectrum in (b) by the factor M in order to get the agreement. The initial values for all points is the same in each case.

Figs. 13 and 15 show spectra for $M = 54$, obtained from the FFT algorithm in (a) and from our analytical expression (Eq. (44)) in (b). The agreement is excellent when the FFT of the map (Eq. (4)) in (b) uses M times the number of points in the FFT in (a). The envelope of this power spectrum decays as $1/\sin^2 f_k$, as can be seen by setting the numerator in Eq. (44) equal to 1 (see Figs. 13 and 15). The low-to-mid frequency part of these spectra, at which most of the energy of the chaotic fluctuations concentrates, then approximately follows a power law $S(f) \simeq 1/f^2$ (as can be seen by Taylor expansion of the denominator in Eq. (44)), a property usually associated with stochastic processes. The spectrum of M parallel maps thus appears as a collection of peaks, whose shape is determined by the spectrum of a single map, and these peaks are "superimposed" on a background similar to a noise background at low-to-mid frequencies.

We note that this decay rate does not depend on the specific map (Ikeda or Mackey–Glass) obtained in the singular limit. This map only determines the shape of the peaks in the CTDE limit.

There is also a correspondence, for large delays, between the peaks in these CTDE spectra with the mode frequencies in the DDE: $f_n^{\mathrm{DDE}} = n/2\tau$ ($n = 1, 3, 5, \ldots, [\tau/\Delta] + 1$) for the DDE, and $f_n^{\mathrm{CTDE}} = n/2M\Delta (n = 1, 3, 5, \ldots, (M + 1))$, where $M = [\tau/\Delta]$. [ ] stands for the integer part of τ/Δ. Δ is the sampling time in the DDE. In the CTDE the frequencies should be estimated in the middle of the main peaks. The attractor dimension can then be found from the CTDE by counting the number of peaks within $c\delta^{-1}\Delta$. For DDEs at large delay, these estimates agree with the $c\delta^{-1}\tau$ estimate proposed in [5].

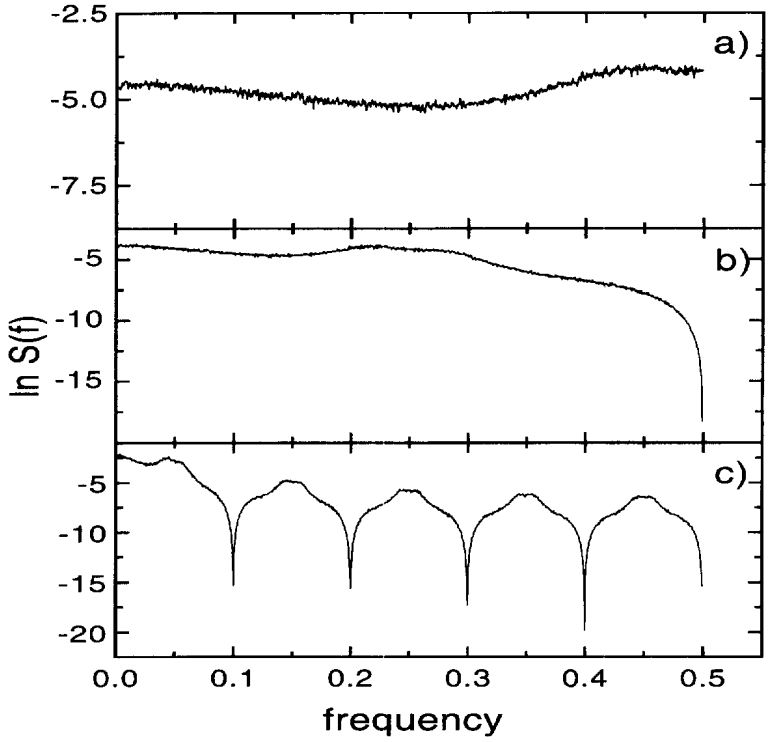

Fig. 14. Power spectra of the Ikeda CTDE $x(t) = 2.1b^{-1}\pi \sin(x(t-\tau))$ with parameters $b = 1$ and $\tau = 20$: (a) power spectrum for $M = 1$, i.e. for a single point evolving according to the Ikeda map: (b) Same as in (a) but $M = 2$; (c) same as in (a) but $M = 10$. The initial values for all points is the same in each case.

6. Conclusion

In conclusion, the peaks in the power spectra of the Mackey–Glass and Ikeda models at large delays are found to agree with the frequencies of the linear modes obtained through linear stability analysis of the dynamics around the fixed point. The attractor dimension can be estimated from the power spectrum of the DDE using these peaks; it can also be estimated using the CTDE approach (Eq. (44)) combined with the numerically determined spectrum from a single map (Eq. (4)); hence our approach to calculating dimension (and metric entropy) is simpler than the one based on the computation of Lyapunov exponents. We anticipate that our results may be applicable to DDEs other than the simple first-order ones of the type studied here.

The map (Eq. (4)) obtained in the singular limit of the Mackey–Glass DDE explains many properties of the DDE. For example, this map exhibits a period-doubling cascade to chaos like the DDE. This is not the case for all DDEs. LeBerre et al. [4] have shown that the bifurcation sequence to chaos in the ring-cavity DDE is different from that of the two-dimensional map obtained in its singular limit, even though the Lyapunov dimension increases linearly with the delay as for the Mackey–Glass equation. In particular, they show that the dimension of attractors in the "map" description is bounded by the dimension of the map, i.e. 2. Our approach here suggests that the CTDE is perhaps a better system with which to compare attractor dimensions of DDEs. The CTDE is in fact infinite-dimensional, as is the DDE from which it is derived as the delay (or more precisely, the ratio R) becomes infinite.

Farmer [2] suggested that the number of degrees of freedom in the DDE is likely to be related to the embedding dimension of the attractor rather than to its Lyapunov or information dimension. Alternately, LeBerre et al. [4] have

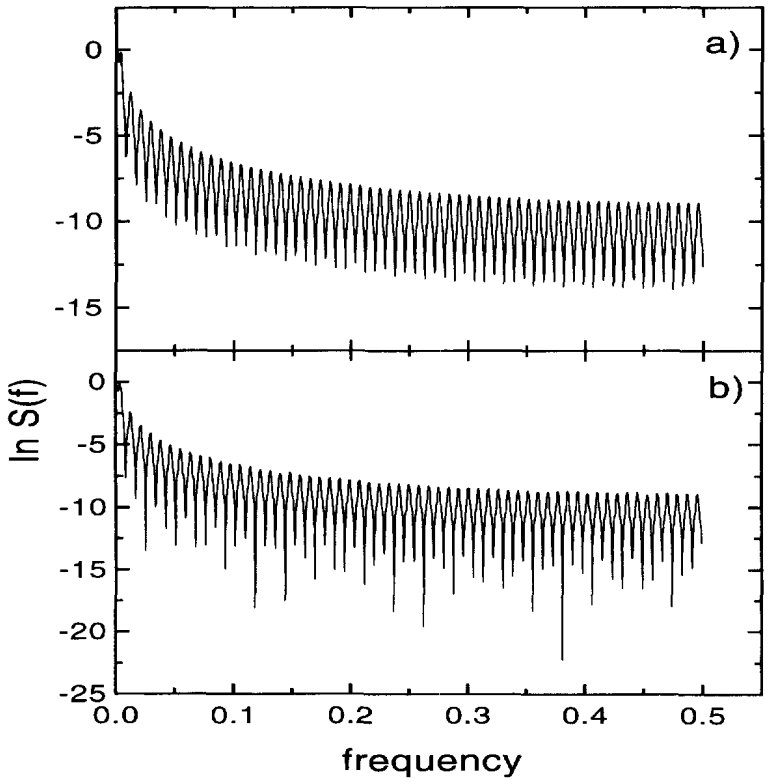

Fig. 15. Power spectra of the Ikeda CTDE with $M = 118$, calculated (a) from the time series generated by the CTDE, and (b) analytically using Eq. (50) in which $S_1(f_k)$ is the power spectrum computed numerically from the evolution of a single point ($M = 1$) (shown in Fig. 14(a)). The initial values for all points is the same in each case.

proposed that the number of degrees of freedom in a laser system such as the ring-cavity system is roughly given by the delay-to-response time ratio $R = \gamma\tau$ for that system (γ is the linewidth). Our findings for the class of first-order DDEs studied here show that the number of modes within the characteristic time δ/c is close to previously reported Lyapunov dimensions, a result in the same spirit as [4].

We summarize our findings as follows:

1. Many properties of the DDE at large delay, such as its dynamical invariants and its power spectra, are related to the roots of the characteristic equation of the DDE, obtained by linearizing its dynamics around the fixed point.
2. The almost-periodic peaks in the power spectrum seen, e.g. for $\tau = 200$ ($R = 20$), first observed by Farmer [2], correspond to the frequencies of the roots of the linearized dynamics. The correspondence becomes perfect as $R \to \infty$. These peaks, corresponding to modes of oscillation, are located at odd integer multiples of the fundamental period which is on the order of 2τ.
3. The disappearance of the modulation in the power spectrum at very large R values follows from the accompanying decrease of the real part of the eigenvalues of the linearized problem.
4. The Lyapunov dimension of the attractor agrees with the number of peaks in the power spectrum between zero frequency and the reciprocal of the correlation time of the feedback function.
5. The sum of the positive Lyapunov exponents equals the rate of decay of the power spectrum in the mid-to-high frequency region (2). This metric entropy stays approximately constant for $R > 5$.

6. Systems with a distribution of delays rather than a single fixed delay exhibit spectral behaviors similar to those of DDEs when their memory kernel becomes sharply localized in time. In particular, when they are equivalent to 200 or more coupled ODEs, the decay rate of their power spectrum is very close to that for the corresponding DDE. Hence our study with distributed delays shows that the decay rates, and thus the attractor dimensions, match only when the system of ODEs for the distributed delay case has sufficient (and very high) dimensionality.
7. The spectra of CTDE can be calculated analytically for piecewise constant initial functions, provided the spectrum of the map obtained in the singular limit is known. This latter spectrum can be obtained numerically. The CTDE spectrum is in fact constructed by translations of the basic spectrum of the map, as well as of mirror symmetric images of this basic spectrum. These basic "units" are then put end to end and multiplied by a filtering function, Eq. (39). As for the DDE at very large delay, the peaks in the CTDE obtained using a large number of plateaus (i.e. for M large) merge, and their fine structure becomes washed out.
8. CTDE spectra for constant initial functions have a particularly simple form (Eq. (44): see Figs. 13 and 15), with the basic peak structure similar to that seen in DDEs at low frequency (see e.g. Fig. 1(b)). That such a correspondence should exist at low-frequency is expected since that is where the behavior of finite-delay DDEs is most similar to that of the CTDE (see Section 2.1). We note that the CTDE spectral decay is very different from that of the DDE, i.e. the singular limit does not produce a smooth transition in the spectra shapes from DDE to CTDE.
9. The peak structure mentioned in the previous item is determined by the spectrum of the map (see Fig. 13(a) for Mackey–Glass and Fig. 15(a) for Ikeda) obtained in the singular limit of the DDE. It is in fact composed of that spectrum alongside its mirror image. This explains why the peaks in the spectrum of the Ikeda DDE are sharp, while those for the Mackey–Glass DDE are broader and have more than one extremum.
10. The more negative Lyapunov exponents can be estimated from the analytical expression for the stable modes, as suggested by Ikeda [3].
11. At very large delays, there is a transition from an exponential to a $1/\sin^2(f)$-type spectrum, which is of $1/f^2$-type at low-to-mid frequencies.

Acknowledgements

This research was supported by NSERC Canada as well as by a CIDA fellowship to BM.

References

[1] V. Kolmanovskii and A. Myshkis, Applied Theory of Functional Differential Equations, Mathematics and its Applications, Vol. 85 (Kluwer Academic Publishers, Dordrecht, 1992).
[2] J.D. Farmer, Chaotic attractor of an infinite-dimensional dynamical system, Physica D 4 (1982) 366.
[3] K. Ikeda and K. Matsumoto, Study of a high-dimensional chaotic attractor, J. Stat. Phys. 44 (1986) 955.
[4] M. LeBerre, E. Ressayre, A. Tallet and H.M. Gibbs, High-dimension chaotic attractors of a nonlinear ring cavity, Phys. Rev. Lett. 56 (1986) 274.
[5] M. Le Berre, E. Ressayre, A. Tallet, H.M. Gibbs, D.L. Kaplan and M.H. Rose, Conjecture on the dimensions of chaotic attractors of delayed-feedback dynamical systems, Phys. Rev. A 35 (1987) 4020.
[6] K. Ikeda and K. Matsumoto, High-dimensional chaotic behavior in systems with time-delayed feedback, Physica D 29 (1987) 223.
[7] S.N. Chow and J. Mallet-Paret, Singularly perturbed delay-differential equations, in: Coupled Nonlinear Oscillators, eds. J. Chandra and A.C. Scott (North-Holland, Amesterdam, 1983) pp. 7–12.
[8] A.F. Ivanov and A.N. Sharkovskii, in: Dynamics Reported, eds. H.O. Walther and U. Kirchgraber, Vol. 3 (Springer, Berlin, 1991) pp. 165–220.
[9] S. Lepri, G. Giacomelli, A. Politi and F.T. Arecchi, High-dimensional chaos in delayed dynamical systems, Physica D 70 (1993) 235.

[10] J. Losson and M.C. Mackey, J. Stat. Phys. 69 (1992) 1025.
[11] G. Giacomelli, R. Meucci, A. Politi and F.T. Arecchi, Defects and spacelike properties of delayed dynamical systems, Phys. Rev. Lett. 73 (1994) 1099.
[12] K. Ikeda, K. Kondo and O. Akimoto, Successive higher-harmonic bifurcations in systems with delayed feedback, Phys. Rev. Lett. 49 (1982) 1467.
[13] T. Aida and P. Davis, IEEE J. Quantum Electron. 28 (1992) 686.
[14] J. Foss, A. Longtin, B. Mensour and J. Milton, Multistability and delayed recurrent loops, Phys. Rev. Lett. 76 (1996) 708.
[15] B. Mensour and A. Longtin, Controlling chaos to store information in delay-differential equations, Phys. Lett. A 205 (1995) 18.
[16] D.E. Sigeti, Exponential decay of power spectra at high frequency and positive Lyapunov exponents, Physica D 82 (1995) 136.
[17] C.G. Lange and R.M. Miura, Singular perturbation analysis of boundary-value problems for differential-difference equations, SIAM J. Appl. Math. 42 (1982) 502.
[18] M.C. Mackey and L. Glass, Oscillation and chaos in physiological control systems, Science 197 (1977) 287.
[19] P. Nardone, P. Mandel and R. Kapral, Analysis of a delay-differential equation in optical bistability, Phys. Rev. A 33 (1986) 2465.
[20] J.Y. Gao, L.M. Narducci, L.S. Schulman, M. Squicciarini and J.M. Yuan, Route to chaos in a hybrid bistable system with delay, Phys. Rev. A 28 (1983) 2910.
[21] K. Ikeda, H. Daido and O. Akimoto, Optical turbulence: Chaotic behavior of transmitted light from a ring cavity, Phys. Rev. Lett. 45 (1980) 709.
[22] Ya.B. Pesin, Russian Math. Surveys 32 (1977) 55.
[23] D. Ruelle, Chaotic Evolution and Strange Attractors (Cambridge University Press, Cambridge, 1989).
[24] D. Fargue, Réductibilité des systèmes héréditaires à des systèmes dynamiques (régis par des équations différentielles aux dérivées partielles), C. R. Acad. Sci. Paris T. 277, No. 17 (Série B, 2e semestre) (1973) 471.
[25] K.L. Cooke and Z. Grossman, Discrete delay, distributed delay and stability switches, J. Math. Anal. Appl. 86 (1982) 592.